



# Investigations on thermal debinding process for fine 316L stainless steel feedstocks and identification of kinetic parameters from coupling experiments and finite element simulations

Mamen Belgacem <sup>a</sup>, Barriere Thierry <sup>b,\*</sup>, Gelin Jean-Claude <sup>b</sup>

<sup>a</sup> University of Franche-Comté, FEMTO-ST Institute, Besançon, France

<sup>b</sup> University of Franche-Comté, Besançon, France

## ARTICLE INFO

### Article history:

Received 11 May 2012

Received in revised form 25 September 2012

Accepted 6 October 2012

Available online 16 October 2012

### Keywords:

Powder injection moulding

Thermal debinding

Kinetic parameters

Numerical simulation

Porous media

Binder distribution

## ABSTRACT

Thermal debinding is one of the most important steps in powder injection moulding process. Thermogravimetric analysis (TGA) was employed to analyze thermal debinding behaviour under argon atmosphere. Thermal debinding kinetics with different heating rates have been compared using 316L stainless steel feedstocks loaded typically at 60, 62, 64 and 66 vol.% for fine metallic powders  $D_{50} = 3.4 \mu\text{m}$ . The Kissinger and Ozawa methods have been used to estimate the kinetic parameters from thermogravimetric experiments. To set up the numerical simulations of thermal debinding stage using finite element methods, a coupled mathematical model for mass diffusion and heat transfer in deformable porous media have been developed. The basic steps of the proposed model consist of solving the following coupled problems: thermal degradation of binder coupled with heat transfer and deformation phenomena by finite element methods using Comsol Multiphysics® software. The obtained numerical simulation results are in proper agreement with experimental data. The proposed numerical simulations allow the determination of remaining binder distribution, temperature distribution and deformation fields in the component during the whole thermal debinding process at any time.

© 2012 Elsevier B.V. All rights reserved.

## 1. Introduction

Powder injection moulding (PIM) is an established, net or near-net shape process which is used for the cost-effective mass production of metallic or ceramic components. It combines the design flexibility of plastic injection moulding and the advantage of powder metallurgy of nearly unlimited choice of material [1]. The PIM processing includes four stages: mixing of very fine metallic or ceramic powders and thermoplastic binders to elaborate a feedstock, injection of powder/binder mixtures in the cavity die mould, thermal/catalytic or solvent debinding stage and finally sintering by solid state diffusion [2]. The binder system usually consists of several components, which have different functionalities. First binder paraffin wax (PW) has a low viscosity to allow an easy cavity filling during injection moulding. The second binder is polypropylene (PP) that keeps the component shape after injection moulding and then debinding. The third binder is an additive surfactant stearic acid (SA) that is added to facilitate powder wetting by decreasing the surface energy of the binder-powder [3].

Thermoplastic binders are widely used both in powder metallurgy or ceramic industries, such as in sensors manufacturing and medical devices [4]. Such binders need to be removed from the powder compact before the sintering stage at final functional component. The most

commonly used method of binder removal is thermal debinding, which is simply the oxidation of the binder in air or the pyrolysis of binder in argon. If binder removal is incomplete, the trapped polymeric residues will be a contamination source and may affect the final physical or electrical properties of the component [5]. If the binder removal is too fast, defects such as cracks and large voids may appear and will affect the micro-structural characteristics of the component during sintering [6]. The successful removal of binder occurs without disrupting the packing of the particles or producing any defects in the green components. Thus, the thermal debinding is a critical processing step in the powder injection moulding for processing microcomponents [7].

Thermal stability studies of different materials by differential thermal analysis (DTA) and thermogravimetric analysis (TGA) have been carried out during years [8]. Kinetic studies are a main aspect in thermal analysis, in which the purpose is to determine the pyrolysis reaction mechanism and to identify the parameters of the Arrhenius equation [9]. Kissinger [10] and Ozawa [11] methods demonstrated that DTA, based on the linear relation between peak temperature and heating rate, can be used to determine the main kinetic parameters of the thermal decomposition: activation energy ( $E$ ) and pre-exponential factor ( $A$ ).

G. Aggarwal et al. proposed a mathematical model based on the fundamental characteristics of the polymeric binders used in PIM. The model can predict the decomposition behaviour for new binder formulations related to different powder characteristics. It provides a tool to conveniently change the binder formulations with or without metal

\* Corresponding author. Tel.: +33 3 81 66 60 75.

E-mail address: [thierry.barriere@ens2m.fr](mailto:thierry.barriere@ens2m.fr) (B. Thiery).

powder and to calculate the degradation temperature, the holding time and the heating rate for the debinding process. An earlier study has been proposed for degradation of binders used in powder injection moulding for the manufacturing of complex shape in titanium and Ti alloys [12]. A comprehensive approach based on intrinsic kinetics of polymers pyrolysis has been set-up to formulate a master decomposition curve (MDC) for each individual binder component and found to be very useful for systematic analyses of thermal debinding behaviours [13].

During the last recent years, 316L stainless steel is one of the most common metals for injection moulding, either provided in gas atomized or water atomized. Its popularity results from its capabilities to be sintered to high densities and its corrosion resistance [14]. A large number of researchers investigated the different aspects of 316L stainless steel. Raza et al. related that the thermal debinding temperature, heating rate and thermal debinding time can considerably influence the final characteristics of PIM products [15]. Barriere et al. conclude that particle size, shape, solid loading, heating rate and atmosphere also affect the deformation defects [16].

The purpose of this study has been to investigate the influence of powder volume loading on thermal debinding behaviour of the feedstocks based on 316L fine stainless steel powders ( $D_{50} = 3.4 \mu\text{m}$ ) and a multi-component binder system. A kinetic model, based on the kinetic parameters ( $E$  and  $A$ ) of polymer pyrolysis, has been proposed in our study for a multi-reaction steps. Therefore, the activation energy has been calculated from experiments and the pre-exponential factor has been identified using an inverse identification strategy, by the mean of the quadratic error estimation. Then the kinetic parameters are used in an appropriate finite element model in order to perform the simulation of thermal debinding process for 2D and 3D bending test specimens. The proposed numerical simulations allow the determination of the remaining binder distribution, temperature distribution and deformation fields in the component during the whole thermal debinding process at any time.

## 2. Kinetic model for multi-reaction steps

This proposed model is developed for the purpose of describing the TGA curves which exhibit two decomposition steps. The first step corresponds to the decomposition of stearic acid and paraffin wax and the second one corresponds to the decomposition of polypropylene. All kinetic analyses assume that the isothermal rate of conversion is a linear function of a temperature-dependent rate constant ( $k$ ) and a temperature-independent function of the conversion [17], the remaining weight fraction of a polymer ( $C_b$ ) can be expressed as:

$$dC_b/dt = k \cdot f(C_b) \quad (1)$$

where  $k$  is the rate constant for thermal degradation ( $\text{min}^{-1}$ ) that follows an Arrhenius equation. The kinetic function of the thermal decomposition is defined in Eq. (2) in which ( $n$ ) is the apparent reaction order and is assumed to be constant during the greater part of the reaction [18].

$$f(C_b) = (1 - C_b)^n = (1 - C_b) \quad (2)$$

The Arrhenius equation is given as:

$$k = Ae^{-E/RT} \quad (3)$$

where  $A$  is the pre-exponential factor assumed to be temperature independent ( $\text{min}^{-1}$ ),  $E$  is the activation energy for thermal degradation ( $\text{J mol}^{-1}$ ),  $R$  is the gas constant ( $\text{J mol}^{-1} \text{K}^{-1}$ ) and  $T$  is the absolute temperature.

Metal powders may have catalytic effects on the pyrolysis rate. However, the shape of the pyrolysis curve with powders is similar

to that without powders [12]. Therefore, Eq. (3) of polymer pyrolysis can still be applied for feedstocks [13]:

$$C_b = wC_{b1} + (1-w)C_{b2} \quad (4)$$

$$w = C_{01}/(C_{01} + C_{02}) \quad (5)$$

$$C_0 = C_{01} + C_{02} \quad (6)$$

where  $C_b$  is the mass ratio corresponding to the mass of both polymers where  $C_{b1}$  is the mass ratio to initial mass of the low molecular weight polymer and  $C_{b2}$  the mass ratio to the initial mass of the high molecular weight polymer,  $C_0$  is the initial mass of the two polymers  $w$  is the ratio of the initial mass of the low molecular weight polymer to the initial mass of the two polymers,  $C_{01}$  and  $C_{02}$  initial mass of low molecular and high molecular weight polymer, respectively. In our case, SA and PW have low molecular weight and PP has high molecular weight (Table 2).

If the sample temperature is changed at a controlled and constant heating rate  $\beta$ , the variation in the conversion can be analyzed as a function of temperature, this temperature being dependent on the time of heating. Therefore, the reaction rate may be written as follows:

$$dT = \beta dt \quad (7)$$

$$dC_b/dt = \beta dC_b/dT \quad (8)$$

Substituting expressions (8), (3) and (2) into Eq. (1) gives the expression of the reaction rate in the form:

$$dC_b/dT = (A_i/\beta)e^{-E_i/RT}(1 - C_b) \quad (9)$$

where  $A_i$  and  $E_i$  are the kinetic parameters for each step.

## 3. Experiments and methodologies

### 3.1. Powder and binder characteristics

The fine metallic powders used in this analysis consist in a gas atomized spherical stainless 316L steel powders with a density equals  $7.9 \text{ g/cm}^3$  [19]. Table 1 indicates the powder size distribution and the chemical composition. Fig. 1 exhibits a scanning electron micrograph (SEM) of the used powders. One can notice that most of particles are mainly spherical or elliptical, that is well appropriated for injection moulding. A multi-component binder system based on paraffin wax has been prepared and used. The primary binder polypropylene (PP) has been chosen to keep the component shape after injection moulding and then debinding. The paraffin wax (PW) has been chosen as the secondary binder in order to decrease the feedstock viscosity to allow an easy flow during injection moulding. The additive surfactant stearic acid (SA) has been added to facilitate powder wetting. The characteristics of the binder components are summarized in Table 2. The 316L stainless steel powders mixture with different powder volume loadings varying 60 to 66% with

**Table 1**

Particle size distribution and chemical composition of the gas atomized 316L stainless steel powders.

Powder and density									
Powder	Size	D <sub>10</sub>	D <sub>50</sub>	D <sub>90</sub>	Density				
316L	5 $\mu\text{m}$	1.8 $\mu\text{m}$	3.4 $\mu\text{m}$	6.0 $\mu\text{m}$	7.9 $\text{g} \cdot \text{cm}^{-3}$				
Powder chemical composition									
Element	Cr	Ni	Mo	Mn	Si	C	P	S	Fe
wt.%	17.4	10.9	2.5	1.2	1.64	0.021	0.015	0.0006	Bal.

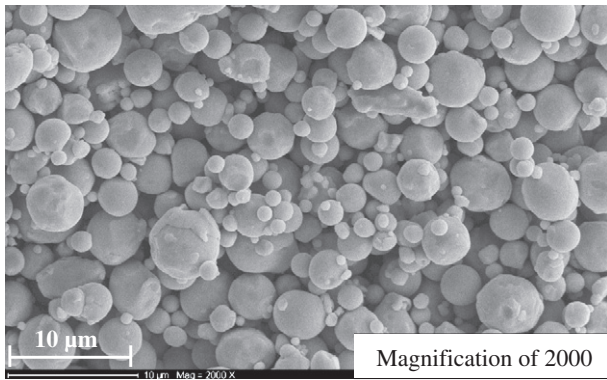


Fig. 1. Scanning electron micrographs of fine 316L stainless steel powders ( $D_{50} = 3.4 \mu\text{m}$ ) used in the proposed investigations with magnification equals 2000.

increment 2% has been then mixed with the polymeric binder at a temperature equals 160 °C during 30 min with twin screw mixing.

### 3.2. Feedstock thermal decomposition measurement

The debinding process has been carried out by thermal debinding using thermogravimetric analysis (TGA) and differential thermal analysis (DTG) SETSYS Evolution provided by Setaram®. The temperature test varied from 25 to 500 °C at three different heating rates 2, 5 and 10 °C/min for elaborated feedstocks. To maintain pyrolysis conditions, high purity argon 20 mL/min has been used as the carrier gas to maintain a stable environment. Sample weight was about 100 mg and all the samples have been put and heated in Platinum crucible. The TGA curves for the feedstock loaded at 60% are displayed in Fig. 2(a). The TGA curves exhibit two decomposition steps; the first step in the range from 180 to 350 °C corresponds to the decomposition of stearic acid and paraffin wax according to their low molecular weight. The second one in the range from 350 °C to 460 °C corresponds to the decomposition of polypropylene with high molecular weight. However to analyze thermal debinding, it is important to get accurate maximal decomposition temperature for both steps. DTG results Fig. 2(b) are used to obtain the derivative curve peaks in order to identify the accurate maximal temperature for which polymers are completely degraded. The TG analyses were repeated three times and similar results were obtained.

### 3.3. Estimation of kinetic parameters

In this work the activation energy has been obtained from non-isothermal TGA test. The methods used to calculate kinetic parameters, proposed by Kissinger [10] and Ozawa [11] are called model-free non-isothermal methods and require a set of experimental tests at different heating rates. The activation energy determined by applying these methods is the sum of activation energies associated to chemical

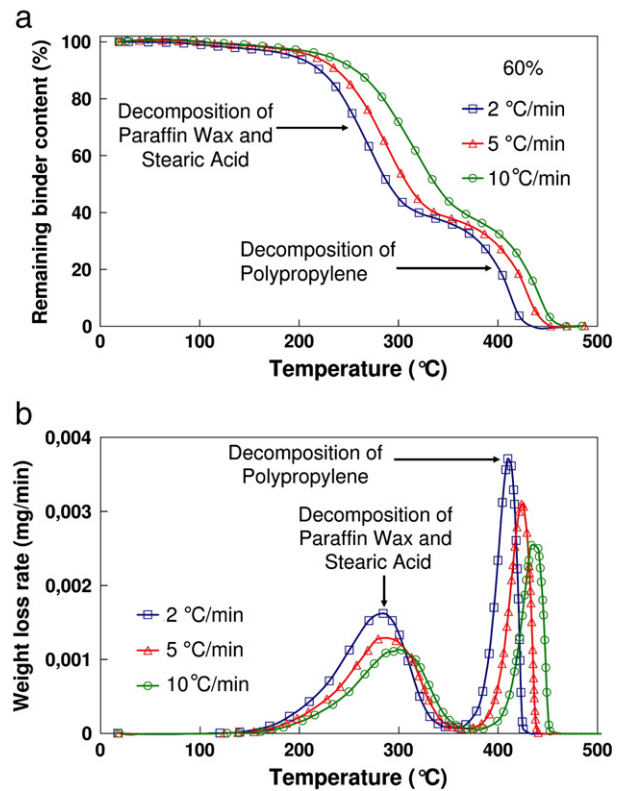


Fig. 2. (a) Remaining binder content curves vs. temperature, (b) weight binder loss rate curves vs. temperature corresponding to a powder volume loading equals to 60% at different heating rates for 316L stainless steel in argon atmosphere.

reactions and physical processes in thermal decomposition and therefore it is called apparent activation energy [20].

#### 3.3.1. Ozawa method

The Ozawa method [21] allows obtaining the apparent activation energy ( $E$ ) from a plot of common logarithm of heating rates,  $\log \beta$ , versus  $1/T_{\text{max}}$ , which represents the linear relation with a given conversion value at different heating rates.

$$E = -2.19R \left( d \log \beta / dT_{\text{max}}^{-1} \right) \quad (10)$$

#### 3.3.2. Kissinger method

This method allows obtaining the kinetic parameters of a solid-state reaction without knowing the reaction mechanism. Kissinger [22] has developed a non isothermal method where there is no need to calculate ( $E$ ) for each conversion value in order to evaluate kinetic parameters.

Table 2

Characteristics of the polymer ingredients used in the binder system.

Binder components	Density [ $\text{g}\cdot\text{cm}^{-3}$ ]	Weight fraction (%)	Decomposition range (°C)	Linear formula	Molecular weight
Primary binder	0.90	16	390 to 500	$[\text{CH}_2\text{CH}(\text{CH}_3)]_n$	$M_w \approx 304940$ $M_n \approx 46832$
Polypropylene (PP)	0.91	22	260 to 380	$[\text{C}_n\text{H}_{2n+2}]_m$	$M_w \approx 754$ $M_n \approx 721$
Secondary binder	0.86	2	220 to 350	$[\text{CH}_3(\text{CH}_2)_{16}\text{COOH}]$	$M_w \approx 484$ $M_n \approx 475$
Paraffin Wax (PW)					
Surfactant					
Stearic Acid (SA)					
Initial binder content			PW + SA + PP = 40%		
Components	$C_{O1} = \text{PW} + \text{SA}$		$C_{O2} = \text{PP}$		w
Values	24%		16%		0.4

This method allows obtaining the value of activation energy from a plot of  $\ln(\beta/T_{max}^2)$  against  $1/T_{max}$ .

$$E = -R \left[ d \ln \left( \beta / T_{max}^2 \right) / dT_{max}^{-1} \right] \quad (11)$$

Once ( $E$ ) is known, the values of pre-exponential factor,  $A$ , are calculated with Eq. (12):

$$A = \beta E e^{E/RT_{max}} / RT_{max}^2 \quad (12)$$

The correlation between ( $E$ ) and ( $A$ ) observed by Seong-Jin et al. for titanium powder [13] is quite similar to the one observed in the present work.

#### 4. Identification of kinetic parameters and numerical simulation by finite element methods

##### 4.1. Identification of kinetic parameters for a fine 316L stainless steel feedstock

The strategy to identify the kinetic parameters  $A_1$  and  $A_2$  using Matlab® platform consists in fitting the numerical remaining binder content curve according to Eq. (13) to the one obtained from the TGA tests. The inverse identification procedure [23], by the mean of the squared estimation error, has been used as related in the algorithm summarized in the following expression:

$$\begin{cases} \min G(x) \\ G(x) = \sum_{i=1}^n |C_b^{exp}(T_i, x) - C_b^{num}(T_i, x)|^2 \\ x = [A_1, A_2] \end{cases} \quad (13)$$

where  $G(x)$  is the mean residual squares of the tolerance objective function where  $i = 1, \dots, n$  indicates different values of the debinding temperature;  $x$  stands for the set of material parameters to be identified,  $C_b^{exp}$  is the experimental remaining binder content obtained from the TGA test and  $C_b^{num}$  is numerical remaining binder content obtained by using the optimization procedure. Nelder–Mead Simplex method has been employed to minimize the value of  $G(x)$  in our case.

Kinetic parameters should be determined properly and their determination for thermal debinding model is important to obtain accurate results in numerical simulations by finite element methods. The variation of the remaining binder content obtained using the identified kinetic parameters with heating rate 2 °C/min is related in Fig. 3. One can notice that the global average error is about 5%. The inverse method results are in a proper agreement with the experimental ones. The experimental and identified kinetic parameters obtained for a fine 316L

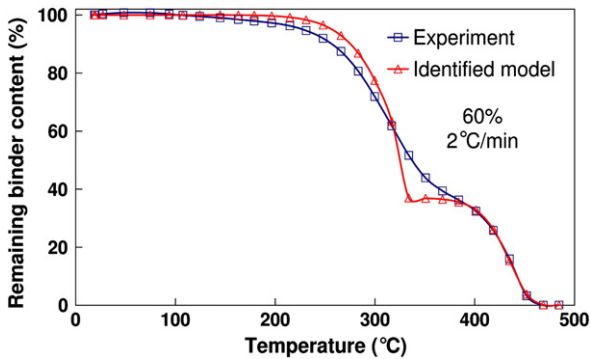


Fig. 3. Evolution of remaining binder content versus temperature, comparison between experimental and identified kinetic model results for a fine 316L stainless steel feedstock loaded at 60% of powder volume loading with heating rate equals 2 °C/min in argon atmosphere.

Table 3

Experimental and identified kinetic parameters for fine 316L stainless steel feedstocks loaded from 60 to 66%.

Methods		Ozawa	Kissinger	
60%	Experimental kinetic parameters	$A_1$ (min <sup>-1</sup> )	$4.24 \times 10^7$	$1.45 \times 10^7$
		$A_2$ (min <sup>-1</sup> )	$1.50 \times 10^{16}$	$1.48 \times 10^{16}$
	Identified kinetic parameters	$A_1$ (min <sup>-1</sup> )	$1.53 \times 10^4$	$0.46 \times 10^4$
		$A_2$ (min <sup>-1</sup> )	$1.79 \times 10^{19}$	$1.77 \times 10^{19}$
62%	Experimental kinetic parameters	$A_1$ (min <sup>-1</sup> )	$3.36 \times 10^6$	$1.01 \times 10^6$
		$A_2$ (min <sup>-1</sup> )	$2.38 \times 10^{12}$	$1.51 \times 10^{12}$
	Identified kinetic parameters	$A_1$ (min <sup>-1</sup> )	$1.47 \times 10^3$	$0.48 \times 10^3$
		$A_2$ (min <sup>-1</sup> )	$2.70 \times 10^{15}$	$1.64 \times 10^{15}$
64%	Experimental kinetic parameters	$A_1$ (min <sup>-1</sup> )	$3.71 \times 10^6$	$1.13 \times 10^6$
		$A_2$ (min <sup>-1</sup> )	$2.21 \times 10^{14}$	$1.69 \times 10^{14}$
	Identified kinetic parameters	$A_1$ (min <sup>-1</sup> )	$1.83 \times 10^3$	$0.54 \times 10^3$
		$A_2$ (min <sup>-1</sup> )	$2.45 \times 10^{17}$	$1.89 \times 10^{17}$
66%	Experimental kinetic parameters	$A_1$ (min <sup>-1</sup> )	$2.02 \times 10^9$	$1.51 \times 10^9$
		$A_2$ (min <sup>-1</sup> )	$9.78 \times 10^{16}$	$9.00 \times 10^{16}$
	Identified kinetic parameters	$A_1$ (min <sup>-1</sup> )	$1.85 \times 10^6$	$0.81 \times 10^6$
		$A_2$ (min <sup>-1</sup> )	$1.52 \times 10^{20}$	$1.49 \times 10^{20}$

stainless steel feedstock loaded at 60%, using both methods Ozawa and Kissinger, are related in Table 3.

##### 4.2. Numerical simulation of thermal debinding using identified kinetic

A 3D model of thermal debinding for which the component behaves as a porous media is assumed. The proposed numerical simulation will be focussed on the second step of debinding process corresponding to degradation of polypropylene (PP). However, the considered deformation during the first debinding step only results from thermal expansion but not from the paraffin wax (PW) and stearic acid (SA) loss. Because even with 24% total loss of paraffin wax and stearic acid, polypropylene (PP) still acts as a backbone to keep the component shape during the first debinding step. So the component deformation during the first debinding step is due only to temperature change. The state equations in the present model are discussed below.

The evolution of the remaining weight binder is governed by the kinetic model, given by Eq. (14):

$$dC_b/dt = k \cdot \nabla^2 C_b, \quad (x, y, z, t) \in \Omega \times [0, t] \quad (14)$$

$$k = Ae^{-E/RT}$$

where  $\Omega$  is the material domain and  $t$  is the time.

The temperature variation is governed by the heat equation, given by Eq. (15):

$$\left( \frac{\phi \cdot \rho_p + C_{02} \cdot \rho_b}{\phi + C_0} \right) \left( \frac{\phi \cdot C_{pp} + C_{02} \cdot C_{pb}}{\phi + C_0} \right) \frac{\partial T(x, y, z, t)}{\partial t} + \text{div}(\vec{q}) = 0, \quad (x, y, z, t) \in \Omega \quad (15)$$

where  $\phi$  is the powder volume loading,  $C_0$  is the initial volume fraction of the binder system,  $C_{02}$  is the volume fraction of the second binder ingredient (PP) polypropylene,  $\rho_p$  is the density of powder skeleton,  $\rho_b$  is the density of polypropylene,  $C_{pp}$  is the specific heat coefficient of powder skeleton and  $C_{pb}$  is the specific heat coefficient of polypropylene.

The Fourier's law gives the relation between the heat flow  $q \rightarrow$  and the temperature  $T$ :

$$\vec{q} = -\lambda \text{grad}(T)$$

where  $\lambda_p, \lambda_b$  are the thermal conduction coefficients of the powder skeleton and polypropylene, respectively. Assuming this relation, the heat equation becomes:

$$\left( \frac{\phi \cdot \lambda_p + C_{02} \cdot \lambda_b}{\phi + C_0} \right) \Delta T = 0, \quad (x, y, z, t) \in \Omega$$

During the final removal of residual polymers from a PIM compact by thermal debinding, two principal

mechanisms contributing to the deformation of the component have been differentiated: polymer-content change and temperature change. Thus, the strain tensor,  $\varepsilon$  describing the deformation of the component is the sum of:

$$\varepsilon = \varepsilon_b + \varepsilon_T + \varepsilon_p \quad (16)$$

where  $\varepsilon_b$  is the deformation caused by polymer-content change,  $\varepsilon_T$  is the deformation caused by temperature change and  $\varepsilon_p$  is the deformation associated to gas pressure. During the polymer-removal process, the powder skeleton is subjected to a body force of distributed load that is equal to the total gas pressure,  $P$ . The partial pressures of polymer vapour effect are taken in account based on the identified kinetic parameters [24].

Using the same methodology as commonly adopted in drying technology [25], the strain caused by polymer-content change and temperature change is considered as follows:

$$\varepsilon = (1 + \nu) \left\{ \left( \frac{\phi \cdot \alpha_p + C_{02} \cdot \alpha_b}{\phi + C_0} \right) \cdot \Delta \frac{C_b}{C_0} \right\} \quad (17)$$

where  $\nu$  is the Poisson's ratio of the powder skeleton,  $\alpha_p$  is the linear-expansion coefficient of powder skeleton and  $\alpha_b$  is the linear-expansion coefficient of polypropylene.

The constitutive behaviour of the powder skeleton is considered to be elastic, as it is dominant for metal powder with a temperature of less than 873 K [24]. It is further assumed that small deformation and low deformation rate are applied. For plane-strain problems, the stress and strain relationship is well defined as [26].

$$\varepsilon = D^{-1} (\sigma - \sigma_0) \quad (18)$$

$D$  is the elasticity matrix, considered to be equal to the sum of the strains caused by polymer-content change and temperature change,  $\sigma$  is the stress tensor and  $\sigma_0$  is the initial residual stress. The initial moulding residual stress has been neglected as the present investigation focuses only on the debinding stage.

The equivalent stress  $\sigma_i$  describes the distortion energy and is responsible for the yielding of a material according to the Huber–von Mises–Hencky criterion, expressed in the following form [27].

$$\sigma_i^2 = 1/6 \left[ (\sigma_x - \sigma_y)^2 + (\sigma_y - \sigma_z)^2 + (\sigma_z - \sigma_x)^2 \right] + \tau_{xy}^2 \quad (19)$$

where  $\sigma_x$ ,  $\sigma_y$ , and  $\sigma_z$  are the stresses in the  $x$ ,  $y$  and  $z$  directions respectively and  $\tau_{xy}$  is the shear stress in the  $xy$  plane.

To illustrate the proposed model and associated numerical scheme, a three-dimensional component with two-dimensional cross section is considered as shown respectively in Fig. 4(a) and (b),  $OA = 15$  mm (long edge),  $OC = 5$  mm (short edge) and  $AD = 0.5$  mm.

#### 4.2.1. Initial and boundary conditions

The solution of the problem requires initial and boundary conditions. Initially, the temperature of the compact is room temperature ( $T_0 = 25$  °C). The initial opened porosity is filled with atmospheric air and its pressure is equal to the ambient pressure of 100,000 Pa.

$$C_b(x, y, z, 0) = C_{02} \quad (x, y, z) \in \Omega$$

$$P(x, y, z, 0) = P_0 = 100000 \text{ Pa}, \quad (x, y, z) \in \Omega$$

$$T(x, y, z, 0) = T_0 = 25^\circ \text{C}, \quad (x, y, z) \in \Omega$$

#### 4.2.2. Boundary conditions

During thermal debinding, two boundary conditions exist, Fig. 4(a). One is the impermeable surfaces, i.e., surfaces OGD A, ABED and OABC,

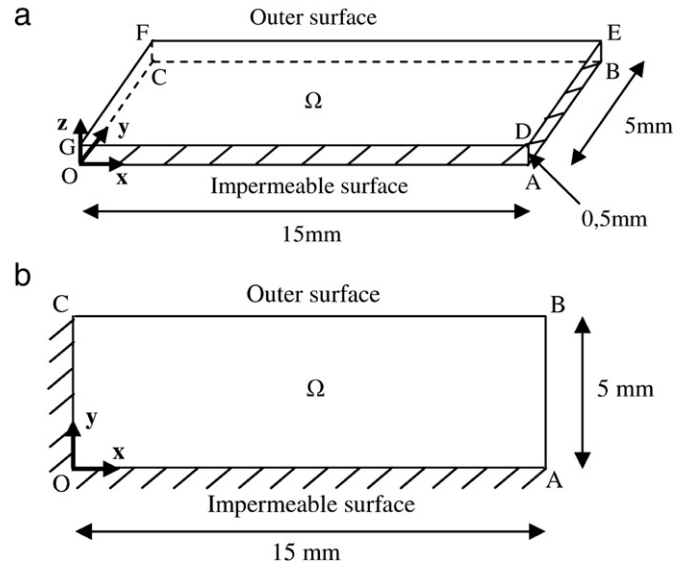


Fig. 4. Description of geometry used for FEM simulations (a) Three-dimensional component with boundaries and (b) two-dimensional cross section of the component.

which are considered to be impermeable and they could be planes of symmetry, where the normal components of heat flux and displacements are zero. The others are the outer surfaces which are exposed to an external field temperature ( $T$ ) as related in Eq. (20). The total gas pressure is equal to the ambient gas pressure.

$$T(x, y, z, t) = T_0 + \beta * t, \quad (x, y, z) \in \partial \Omega_i \quad (20)$$

$$\vec{n} \cdot (\nabla C_b) = 0, \quad (x, y, z) \in \partial \Omega_i$$

where  $\beta$  is the heating rate and  $\vec{n}$  denotes the normal to the boundaries  $\partial \Omega_i$ .

#### 4.3. Material and process numerical implementation

The above governing equations that describe the mass-degradation, thermal problem and deformation phenomena during thermal debinding are strongly coupled, implemented and then solved by finite element methods using Comsol® software. Comsol® is a modelling package for the simulation of any physical process described with partial differential equations (PDE). The coupled kinetic, thermal and mechanical model has been implemented and can be considered as a multiphysic coupled problem between “PDE module” (for degradation problem), “the heat transfer module” (for the thermal problem) and “the structural mechanics module” (for deformation problem), Fig. 5.

The domain  $\Omega$  has been discretized using an automatic mesh generator, with 3560 triangular elements and 1072 quadrilateral elements, resulting in a total of 20,303 degrees of freedom (DOF). An explicit time stepping scheme is used for the time dependant solver algorithm with an automatic time step adjustment. A convergence test, which is not detailed here, validates this mesh choice. The diagram related in Fig. 5 shows the interaction between the three modules. The solution is given at each time step until  $t = t_f$  where  $t_f$  stand for the final processing time. In our analysis,  $t_f$  reach 13,000 s. The material parameters and physical constants used in the present numerical simulation are summarized in Table 4.

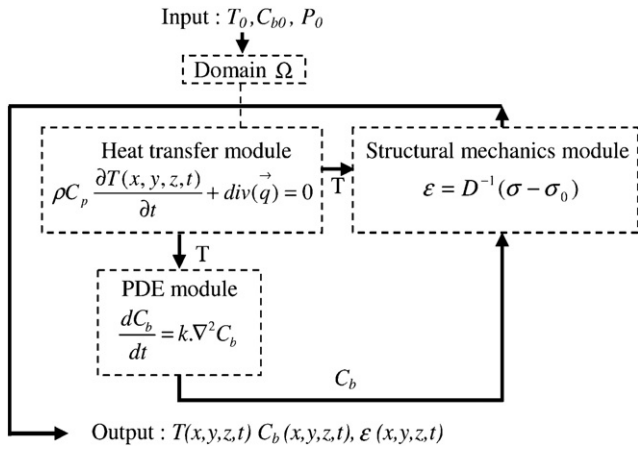


Fig. 5. Interaction diagram between partial differential equations (PDE), heat transfer and structural mechanics module.

5. Results and discussions

5.1. Variation of activation energy during the whole thermal debinding process

Fig. 6 shows the apparent activation energy  $E$  dependencies evaluated for the thermal degradation of different feedstocks loaded typically at 60 to 66% under argon. The initial activation energy required to start degradation was about 80 to 110 kJ mol<sup>-1</sup>. As the reaction approaches 70% conversion, the activation energy increases to a maximum value of about 180 to 235 kJ mol<sup>-1</sup>. This increase falls in the transition region between the first and second step in the mass loss. One can notice that apparent activation energy for the pyrolysis of fine 316L stainless steel feedstocks was not similar for all conversions indicating the existence of a complex multistep mechanism that occurs in the solid state. This means that the thermo-physical mechanism is not the same in the whole degradation process and that activation energy is dependent on conversion and also powder volume loading. A complex dependence of the activation energy on the degree of conversion has been also reported by Budrugaec et al. [28]. Tomašić et al. explained this variation in apparent activation energy in the terms of the heterogeneous nature of solid sample and/or due to a complex reaction mechanism. It is known that degradation reactions are often very complex and can

Table 4  
Conditions for the numerical simulation of thermal debinding process used for a feedstock loaded at 60%.

Model parameters	Value
Binder	PP Polypropylene
Pre-exponential factor	$A = 1.77 \times 10^{19} \text{ min}^{-1}$
Activation energy	$E = 223,92 \text{ kJ/mol}$
Universal gas constant	$R = 8.314 \text{ J/mol}\cdot\text{K}$
Heating rate	$\beta = 2 \text{ }^\circ\text{C/min}$
Ambient pressure	$P_0 = 100,000 \text{ Pa}$
Initial temperature ( $t=0$ )	$T_0 = 25 \text{ }^\circ\text{C}$
Powder volume loading	$\varphi = 60\%$
Linear-expansion coefficient of powder skeleton	$\alpha_p = 18.5 \times 10^{-6} \text{ 1/K}$
Thermal conduction coefficient of powder skeleton	$\lambda_p = 14.6 \text{ W/m}\cdot\text{K}$
Specific heat coefficient of powder skeleton	$C_{pp} = 500 \text{ J/kg}\cdot\text{K}$
Density of powder skeleton	$\rho_p = 7900 \text{ kg/m}^3$
Poisson's ratio of the powder skeleton	$\nu = 0.30$
Total volume fraction of polymer	$C_0 = 40\%$
Volume fraction of polypropylene	$C_{02} = 16\%$
Linear-expansion coefficient of polypropylene	$\alpha_b = 200 \times 10^{-6} \text{ 1/K}$
Thermal conduction coefficient of polypropylene	$\lambda_{pb} = 0.15 \text{ W/m}\cdot\text{K}$
Specific heat coefficient of polypropylene	$C_{pb} = 1800 \text{ J/kg}\cdot\text{K}$
Density of polypropylene	$\rho_b = 900 \text{ kg/m}^3$

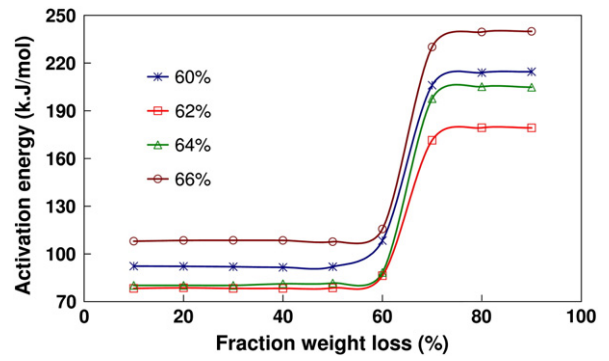


Fig. 6. Apparent activation energy of 316L stainless steel feedstocks as a function of fraction weight loss at different powder volume loadings from 60 to 66% elaborated at the same mixing conditions 160 °C, 30 rpm and 30 min.

involve several processes with different activation energies and physical properties of the considered materials [29].

5.2. Effect of powder volume loading on activation energy

The apparent activation energy of elaborated feedstocks as a function of powder volume loading is shown in Fig. 7. The values of activation energy obtained from the Kissinger method are consistent with the range of values obtained by the Ozawa method and their average values are very near to each other in both steps, which are equal 85.21–90.01 kJ mol<sup>-1</sup> Fig. 7(a) and 212.65–212.91 kJ mol<sup>-1</sup> Fig. 7(b) for Kissinger and Ozawa, respectively. The results related to this investigation are in close agreement with the activation energy value of 214 kJ mol<sup>-1</sup> for 316L stainless material determined by Was et al. in a temperature range from 400 to 500 °C [30]. The relationship between activation energy and pre-exponential factor observed by Seong-Jin et

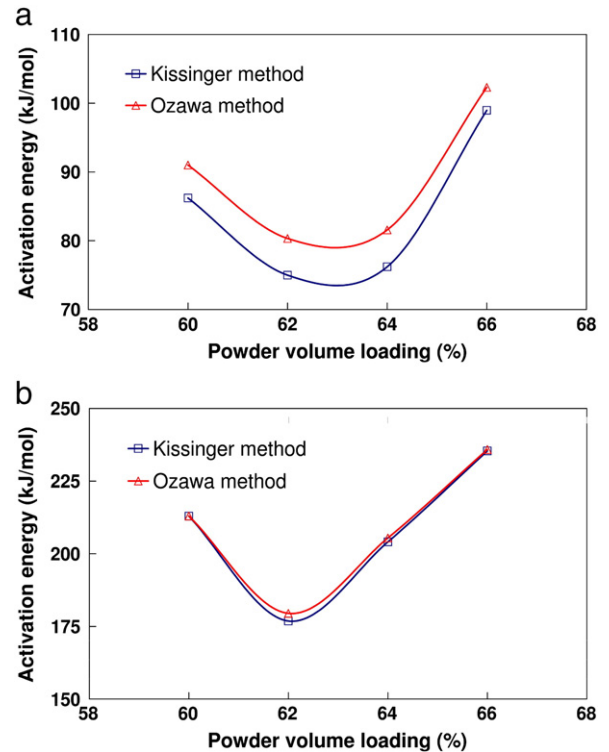
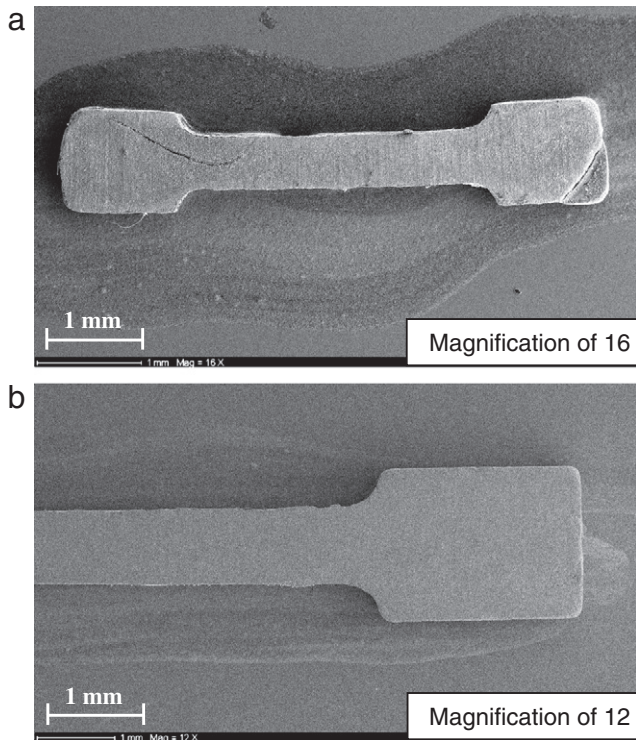


Fig. 7. Apparent activation energy of 316L stainless steel feedstocks (elaborated at the same mixing conditions at 160 °C, 30 rpm and 30 min) as a function of powder volume loading: (a) first step corresponding to degradation of PW + SA, (b) second step corresponding to degradation of PP.



**Fig. 8.** SEM images of debinded tensile specimen after thermal debinding process: (a) feedstock loaded at 66% of powder volume loading and (b) feedstock loaded at 62% of powder volume loading, debound at 300 °C with the same heating rate and the same atmosphere.

al. for titanium powders [13] is quite similar to the one observed in the present work.

The use of different experimental methods for calculations causes that the derived kinetic parameters (even if it were calculated with the same method) may differ for the same type of feedstock. In the related analysis, kinetic parameters obtained from the Kissinger and Ozawa methods for different feedstocks indicate a proper correlation.

The activation energy decreases significantly when powder volume loading ranges from 60% to 62%, then increases more significantly in the range 62–66% as shown in Fig. 7(a) and (b). High value of  $E$  indicates a strong sensitivity of feedstock vs. debinding temperature. Therefore, small temperature fluctuation during thermal debinding for feedstocks with high powder volume loading could cause defects in the debound parts. As debinding temperature increased up to 200 °C, a major change has been noticed associated to debinding rate increasing, as shown previously by the TGA curve in Fig. 2(b). The binder decomposition usually gives an internal gas pressure, if the gas cannot escape fast enough through the interconnected fine pore channels; the gas pressure could

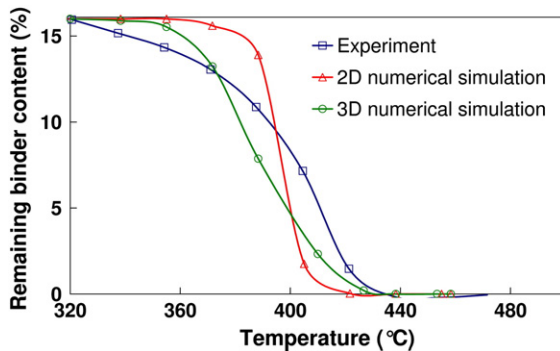


**Fig. 9.** Remaining polypropylene binder content versus debinding temperature for fine 316L stainless steel feedstock loaded at 60% with a heating rate equals 2 °C/min.

increases and build-up [24], particularly in the centre of the part, and tend to push the binder fluid out. If the feedstock is high loaded by powder, the internal gas pressure builds up significantly and leads to the formation of cracks and other defects, as related in the case for feedstock loaded at 66% Fig. 8(a), such cracks and distortions are due to the stress concentration of internal gas pressure in the core of the sample during thermal debinding process. The small value of  $E$  obtained for feedstock loaded at 62% and relatively small for feedstocks loaded in the range 60–64% indicates a low sensitivity to debinding temperature. Consequently, it results that the debinding rate for these feedstocks (larger interconnected pores) becomes less sensitive to heating rates. This allowed a binder system to have a fast debinding rate without introducing high internal stresses from decomposed gas, thereby minimizing stress concentration, cracks and distortions in the debound parts as shown in Fig. 8(b). One can say that feedstock loaded at 62% is the best feedstock to be debound, as this feedstock is less sensitive to temperature.

### 5.3. Numerical simulation results

#### 5.3.1. Mass transport mechanisms related to thermal debinding

Numerical simulations have been carried out on polymer residue distribution during thermal debinding of fine 316L stainless steel powder compact, with a powder volume loading equal to 60%, in order to verify the model. The simulation results are compared with the experimental ones.

Fig. 9 relates the remaining polymer content, obtained from experiments, two-dimensional simulation and three-dimensional simulation, during thermal debinding for fine 316L stainless steel powders bending test specimen. Before the polymer degradation, the rate of polymer removal was very low. The rate of polymer removal increased rapidly as the debinding temperature is already a little above 380 °C, which is

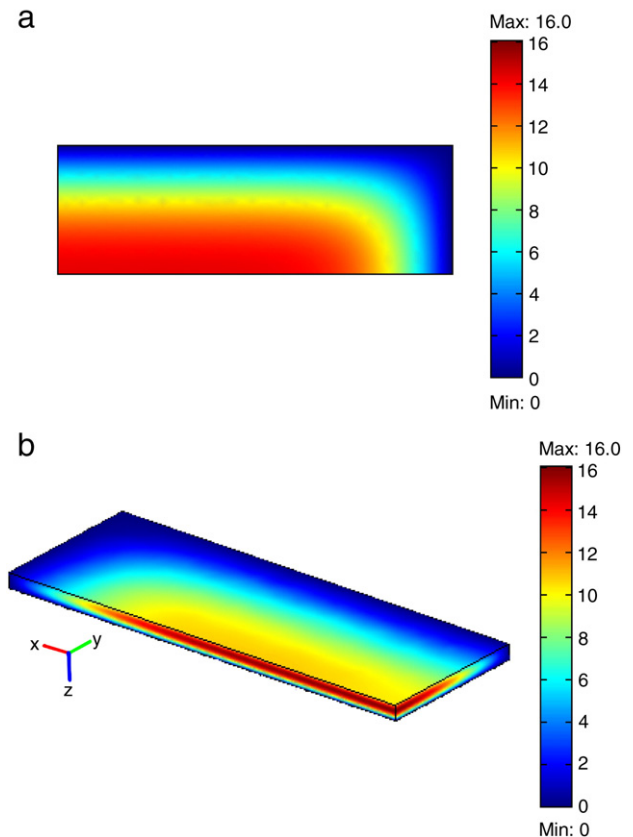


**Fig. 10.** Remaining polypropylene binder content distribution in (%) for fine 316L stainless steel feedstock loaded at 60% with a heating rate equals 2 °C/min at debinding temperature of 385 °C (a) 2D (b) 3D, respectively.

within the degradation temperature range of the polypropylene. When the debinding temperature is around 410 °C, the rate of polymer removal became slow.

The reason is that the limiting debinding rate processing is associated with the diffusion of the polymer rather than with its degradation. Since the diffusion distance for the polymer is short in the initial stage, the debinding rate is quite fast. As debinding proceeds, however, the pore channels extend to the inner region of the compact, and the longer diffusion length slows down the debinding rate. It is clear that the 3D simulation indicates a good agreement with the experimental result than the 2D simulation. This is expected as the 2D simulation ignores some outer surfaces that polymer could escape experimentally when compared with 3D simulation. The 3D simulated results are in proper agreement with the experimental ones.

Fig. 10(a) and (b), 2D and 3D respectively, shows the remaining polypropylene distribution along the width, length and thickness

directions from the centre to the outer surfaces of the compact at the debinding temperature of 385 °C, at which rapid weight loss occurred. The remaining polymer distribution varies continuously with distance from the outer surfaces to the centre of the compact.

Fig. 11(a, b, c) and (d, e, f) presents clearly the remaining binder content profile of different cross sections along the length direction of the component at different debinding temperatures for feedstocks loaded at 60 and 62%, respectively. As can be shown in Fig. 11(a), the remaining binder content in the component is equal to the initial binder content 16% that means there is no degradation of polypropylene at this temperature. Once the imposed temperature reaches the degradation polypropylene temperature as related in Fig. 11(b), the remaining binder is rapidly eliminated at the component surface. This observation implied that the molten polypropylene started migrating towards the external surface. At 425 °C as can be shown in Fig. 11(c), the binder content almost disappeared inside the component and that becomes ready

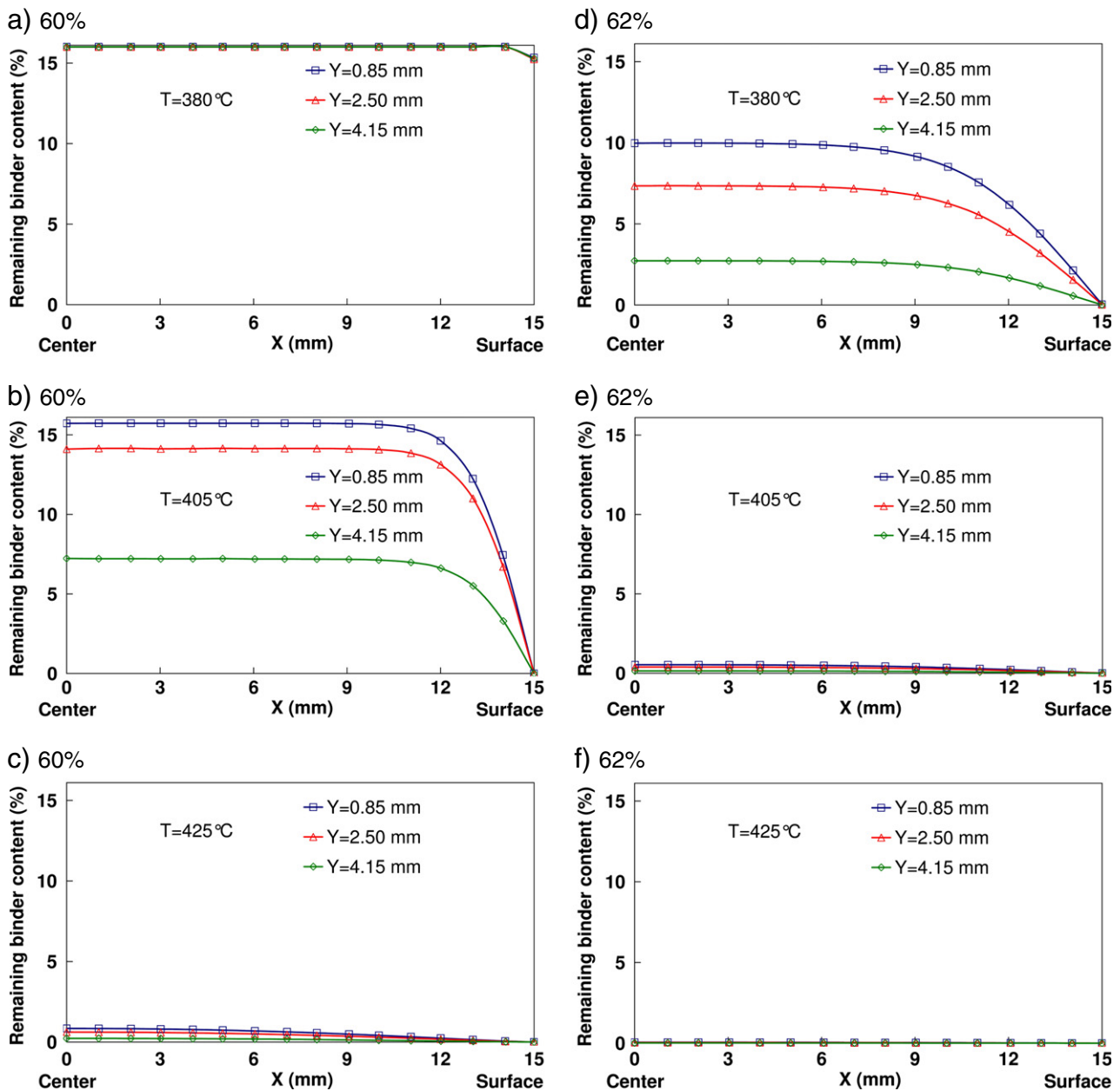


Fig. 11. Predicted distributions of binder content inside the component at different debinding temperatures for fine 316L stainless steel feedstocks loaded at 60 and 62% of powder volume loading.

for the next step which is sintering stage by solid state diffusion. The thermal degradation for feedstock loaded at 62% is much quicker than the 60% one as shown clearly in Fig. 11(d, e, f).

### 5.3.2. Temperature variation inside the PIM component

The temperature evolution at the end of debinding process is shown in Fig. 12(a, b) and (c, d) along the length and the width directions from the center to the outer surface for feedstocks loaded at 60 and 62%, respectively. At the beginning of the simulation, the temperature inside the PIM component is equal to the ambient temperature of 25 °C. During the simulation, the temperature inside the PIM component increases up to a limit value equal to 422 °C, corresponding to the degradation temperature of polypropylene that is used. It is also shown in Fig. 11(a, b, c, d) that there is almost no difference between the temperature at the centre of the component and the outer surfaces where the temperature is practically equal to the imposed furnace one.

### 5.3.3. Geometrical deformation in the PIM component during debinding

Numerical simulations of geometrical deformations in thermal debinding of PIM components, based on the established model, have been carried out. The considered deformations are caused by temperature and binder-content change. The obtained results showed that the dilatations of the PIM component and distortion deformations are principally due to temperature and binder content change, respectively.

Fig. 13(a–b) presents the normal strains and volumetric strain evolution in the PIM component for fine 316L stainless steel feedstocks loaded at 60%. When the temperature varies in the range 25–380°C, compact expands proportionally with temperature, indicating that the thermal expansion of the compact is nearly uniform, and there is almost no shear deformation in the specimen. During the high debinding-rate

period from 380 to 420 °C, the shrinkage caused by polymer removal dominates on the deformation of the compact and the entire specimen contracts as the polymer inside the part is removed rapidly.

Volumetric strains during the thermal debinding stage up to 500 °C with same heating rate of 2 °C/min have been compared for four powder volume loadings 60, 62, 64 and 66%. The maximal total deformations measured for debinded test components range from 2.41 to 2.96% and are illustrated in Fig. 14. In the proposal numerical simulation, a minimum deformation was observed in debinded test specimen loaded at 62%. The results related that deformation was increased considerably at the highest powder volume loading 66%. The difference in deformation is due to the lower volume loading of powders 60 and 62%. The related numerical results are in proper agreement with SEM micrograph results presented in Fig. 8.

## 6. Conclusions

Experimental investigations and numerical simulations related to thermal debinding have been carried out in thermal debinding of metallic components obtained by powder injection moulding of fine 316L stainless steel.

In the first part, the degradation of the fine 316L stainless steel micro-powders mixed with a multi-component binder system has been studied through TGA and DTA analyses under an argon atmosphere. It has been clearly shown that the powder volume loading parameter has an effect on the thermal debinding behaviour. When the feedstock is highly loaded by powder, the high internal gas pressure would build-up significantly and lead to the formation of cracks and other defects as the case for feedstock loaded at 66%. The small value of activation energy obtained for the feedstock loaded at 62% indicates

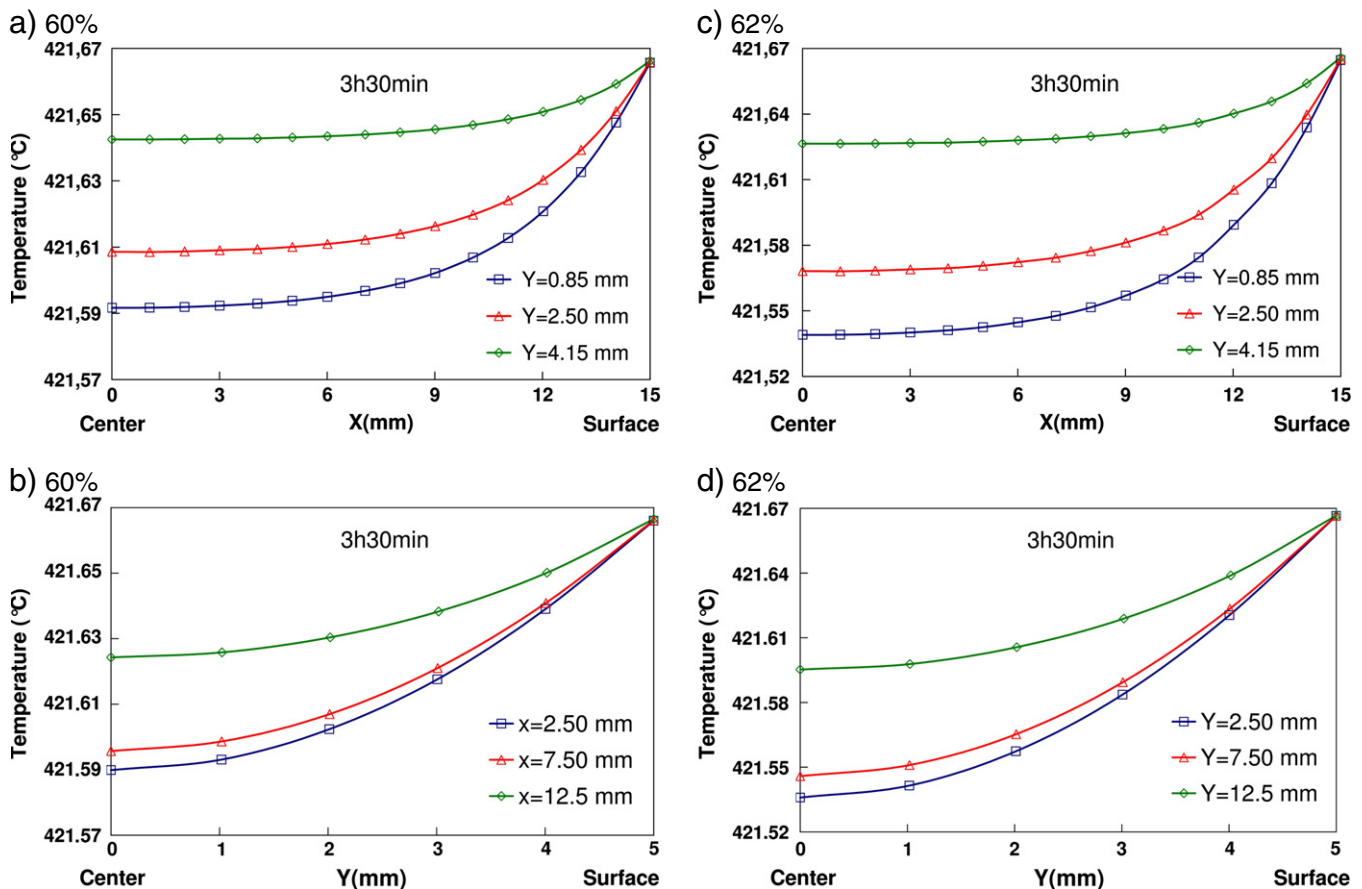


Fig. 12. Temperature distribution in °C at the end of debinding process for fine 316L stainless steel feedstocks loaded at 60 and 62% of powder volume loading, (a)–(c) along the length direction and (b)–(d) along the width direction.

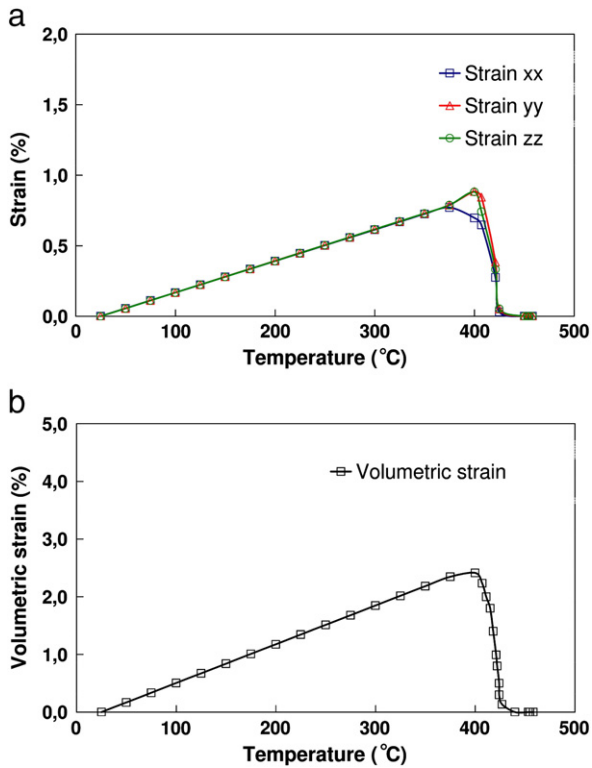


Fig. 13. (a) Normal strains evolution and (b) volumetric strain evolution in the PIM component for fine 316L stainless steel feedstocks loaded at 60%.

that this feedstock is the one less sensitive to temperature (the well adapted for thermal debinding process). The values of the kinetic parameters that have been obtained by the Kissinger and Ozawa methods for different powder volume loadings indicated a proper correlation. One can also conclude that apparent activation energy for the pyrolysis of fine 316L stainless steel feedstocks was not similar for all conversion which indicates the existence of a complex multistep mechanism that occurs at the solid state. This means that the reaction mechanism is not the same in the whole degradation process and that activation energy is dependent on conversion and also powder volume loading.

In the second part, a three-dimensional model of thermal debinding for which the component behaves as a porous media has been established. The kinetic parameters  $A_1$  and  $A_2$  used for fine 316L feedstocks in the present model have been identified in order to fit the numerical remaining binder content curve to the one obtained from the TGA tests, which makes the simulation results more accurate. Using the present model, one can properly analyze the distribution of remaining binder content, temperature and deformation in green components during thermal debinding process.

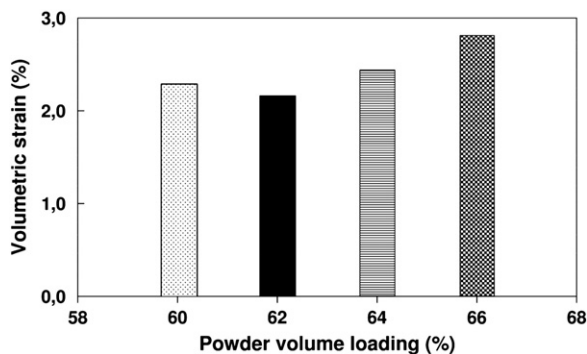


Fig. 14. Volumetric strains in the PIM components with same heating rate of 2 °C/min for different powder volume loadings.

It was shown that the remaining binder content is firstly eliminated at the component surface which means that the molten polypropylene starts to move from the centre towards the external component surfaces.

The present simulation results clearly indicated that the debinding temperature evolution is progressively reached, which guarantees optimal debinding conditions. During thermal debinding, the total deformation of the PIM part is the sum of the deformations caused by polymer-content and temperature change. During the increasing debinding-rate period, the total deformation is caused by temperature evolution and the entire specimen expands. During the high debinding-rate period, the deformation caused by polymer-content change dominates the total deformation of the entire specimen, and the entire specimen contracts. In general, the simulation results are in proper agreement with the experimental ones.

### Acknowledgements

The authors gratefully acknowledge the New PIM project members for funding this research through the FEMTO-ST Institute and ENSMM.

### References

- [1] J. Fleischer, A.M. Dieckmann, Automation of the powder injection molding process, *Journal of Microsystem Technologies* 12 (2006) 702–706.
- [2] B.Y. Tay, N.H. Loh, S.B. Tor, F.L. Ng, G. Fu, X.H. Lu, Characterisation of micro gears produced by micro powder injection moulding, *Journal of Powder Technology* 188 (2009) 179–182.
- [3] B. Mamen, T. Barriere, J.C. Gelin, in: Study of the thermal decomposition for different feedstocks powder injection moulding, *Euro PM2011*, 3, 2011, pp. 235–241.
- [4] M. Imbaby, K. Jiang, I. Chang, Soft lithography and powder metallurgy for fabrication of micro stainless steel machine parts, *Journal of Materials Letters* 62 (2008) 4213–4216.
- [5] S. Masia, P.D. Calvert, W.E. Rhine, H.K. Brown, Effect of oxides on binder burnout during ceramics processing, *Journal of Materials Science* 24 (1989) 1907–1912.
- [6] C. Dong, H.K. Bowen, Hot-stage study of bubble formation during binder burnout, *Journal of the American Ceramic Society* 72 (1989) 1082–1089.
- [7] J.A. Lewis, M.A. Galler, D.P. Bentz, Computer simulations of binder removal from 2-D and 3-D model particulate bodies, *Journal of the American Ceramic Society* 79 (1996) 1377–1388.
- [8] I. Kohsari, S.M. Pourmortazavi, S.S. Hajimirsadeghi, Non-isothermal kinetic study of the thermal decomposition of diaminoxyoxime and diamino furazan, *Journal of Thermal Analysis and Calorimetry* 89 (2007) 543–546.
- [9] S.M. Pourmortazavi, I. Kohsari, M.B. Teimouri, S.S. Hajimirsadeghi, Thermal behaviour kinetic study of dihydroxyoxime and dichloroxyoxime, *Journal of Materials Letters* 61 (2007) 4670–4673.
- [10] H.E. Kissinger, Reaction kinetics in differential thermal analysis, *Journal of Analytical Chemistry* 29 (1957) 1702–1706.
- [11] T. Ozawa, Kinetic analysis of derivative curves in thermal analysis, *Journal of Thermal Analysis* 2 (1970) 301–324.
- [12] G. Aggarwal, S.J. Park, I. Smid, R.M. German, Master decomposition curve for binders used in Powder Injection Molding, *Journal of Metallurgical and Materials Transactions A* 38A (2007) 606–614.
- [13] S.J. Park, Y. Wu, D.F. Heaney, X. Zou, G. Gai, R.M. German, Rheological and thermal debinding behaviors in titanium powder Injection Molding, *Journal of Metallurgical and Materials Transactions A* 40A (2009) 215–222.
- [14] C. Quinard, T. Barriere, J.C. Gelin, Development and property identification of 316L stainless steel feedstock for PIM and  $\mu$ PIM, *Journal of Powder Technology* 190 (2009) 123–128.
- [15] M. Rafi Raza, F. Ahmad, M.A. Omar, R.M. German, Effects of cooling rate on mechanical properties and corrosion resistance of vacuum sintered powder injection molded 316L stainless steel, *Journal of Materials Processing Technology* 212 (2012) 164–170.
- [16] T. Barriere, B. Liu, J.C. Gelin, Determination of the optimal process parameters in metal injection molding from experiments and numerical modeling, *Journal of Materials Processing Technology* 143–144 (2003) 636–644.
- [17] Z. Shi, Z.X. Guo, J.H. Song, A diffusion-controlled kinetic model for binder burnout in a powder compact, *Journal of Acta Materialia* 50 (2002) 1937–1950.
- [18] X. Zhanga, W. Jongb, F. Pretoa, *Journal of Biomass and Bioenergy* 33 (2009) 1435–1441.
- [19] X. Kong, T. Barriere, J.C. Gelin, C. Quinard, Investigations on sintering of 316L stainless steel powders and identification of physical parameters from coupling experiments and finite element simulations, *International Journal Powder Metallurgy* 46 (2010) 61–72.
- [20] M.E.V.S. Suárez-Iha, J.A.F.F. Rocco, J.E.S. Lima, A.G. Frutuoso, K. Iha, M. Ionashiro, J.R. Matos, TG studies of a composite solid rocket propellant based on HTPB-binder, *Journal of Thermal Analysis and Calorimetry* 77 (2004) 803–813.
- [21] T. Ozawa, A new method of analyzing thermo gravimetric data, *Bulletin of the Chemical Society of Japan* 38 (1965) 1881–1886.
- [22] H. Kissinger, Variation of peak temperature with heating rate in differential thermal analysis, *Journal of Research of the National Bureau of Standards* 57 (1956) 217–221.

- [23] J.C. Lagarias, J.A. Reeds, M.H. Wright, P.E. Wright, Convergence properties of the Nelder–mead simplex method in low dimensions, *SIAM Journal on Optimization* 9 (1998) 112–147.
- [24] Y. Shengjie, Y.C. lam, S.C.M. Yu, K.C. Tam, Thermal debinding modeling of mass transport and deformation in powder-injection molding compact, *Journal of Metallurgical and Materials Transactions B* 33B (2002) 477–488.
- [25] S.J. Kowalski, G. Musielak, A. Rybicki, Response of dried materials on drying conditions, *International Journal of Heat and Mass Transfer* 40 (1997) 1217–1226.
- [26] O.C. Zienkiewicz, *The Finite Element Method*, 3rd edition McGraw Hill, London, 1977. [787 pages].
- [27] G. Musielak, Internal stresses caused by outflow of moisture and phase change inside dried material, *Drying Technology* 14 (1996) 289–306.
- [28] P. Budrugaec, E. Segal, On the nonlinear isoconversional procedures to evaluate the activation energy of nonisothermal reactions in solids, *International Journal of Chemical Kinetics* 36 (2004) 87–93.
- [29] V. Tomašić, I. Brnardić, H. Jenei, V. Kosar, S. Zrnèčvić, Combustion of active carbon as a model carbon material: comparison of non-catalytic and catalytic oxidation, *Journal of Chemical & Biochemical Engineering Quarterly* 25 (2011) 283–287.
- [30] G.S. Was, S. Teyseyre, Z. Jiao, Corrosion of Austenitic alloys in supercritical water, *Corrosion Reviews* 62 (2006) 989–1005.